ACS OMEGA

http://pubs.acs.org/journal/acsodf

Article

Dielectric Properties and Flexibility of Polyacrylonitrile/Graphene Oxide Composite Nanofibers

Muhammad Rama Almafie, Leni Marlina, Riyanto Riyanto, Jaidan Jauhari, Zainuddin Nawawi, and Ida Sriyanti*

Cite This: *ACS Omega* 2022, 7, 33087−33096

Read Online

ACCESS | Metrics & More | Article Recommendations

ABSTRACT: Energy storage and modern electronics industries are in essential need of high dielectric and highly flexible materials. In this study, polyacrylonitrile and reduced graphene oxide (PAN/GO) were prepared by electrospinning. The composite morphology produced a homogeneous, smooth, and flexible surface with high tensile strength and durability. The diameter of the fibers in the composite mats ranged from 232 to 592 nm. The X-ray diffraction pattern recording displayed a sharp peak characteristic centered between 20 and 30° angles with a maximum degree of crystallinity of 86.23%. The evaluation of the Fourier-transform infrared spectrum indicated the interaction between GO and PAN through hydrogen bonds. The differential scanning calorimetry measurements confirmed that GO acted as a nucleating agent that improves the thermal stability of the composite. The dielectric properties exhibited the relative permittivity of the composite of 86.4 with a dielectric loss (tan δ) of 4.97 at 10^2 Hz, and the maximum conductivity was achieved at 34.9 × 10^{-6} Sm^{-1} at high frequencies.

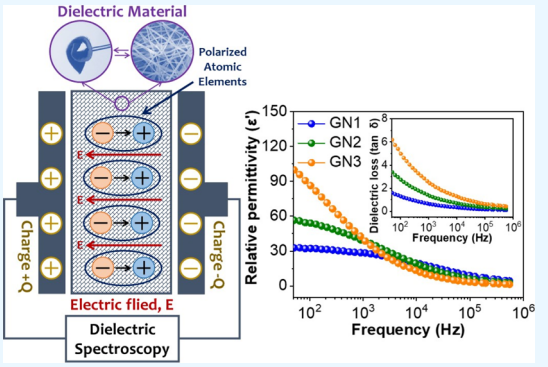

1. INTRODUCTION

Energy storage devices offer an effective solution in overcoming mismatches of and improve the flow of energy between supply and demand.[1,2] To facilitate these conditions, several renewable energy sources were developed, such as bioenergy,[3,4] marine,[5] hydrogen,[2] and fuel cells[1] and capacitors.[6,7] The capacitor in particular is the most popular electricity storage for its high power density and high electric energy charge−discharge.[8,9] This condition is closely related with the material offering the best performance, one of which is the dielectric material. Ideally, the dielectric material has high relative permittivity (ε') and low dielectric loss (tan δ) as the determining factor in increasing energy storage capability.[10,11] Therefore, in recent years, people have been looking for alternative materials that have better and more flexible dielectric properties. This is important to support the development of the electronic trend toward the manufacture of flexible devices, such as flexible screens, flexible cell phones, and wearable devices.

The previously developed approaches that improve the dielectric properties of materials have introduced certain materials having high dielectric properties into polymer composites,[12] incorporating ceramic filler materials with intrinsically high permittivity into the polymer matrix,[13] integrating conductor filling materials into polymeric matrices with metals[14] and semiconductors[15,16] based on the principle of percolation and have also introduced the carbon-based materials.[17] Graphene is a carbon-based material that can be exploited to increase the relative sensitivity of polymers.[18] This carbon allotropy provides outstanding mechanical, electrical, and thermal features. Graphene oxide nanosheets anticipate the increase of the electrical conductivity of polymers by creating a conductivity network close to the percolation threshold while maintaining reasonable processability of the original polymer matrix.[9]

Graphene oxide is employed constantly by researchers to increase the relative permittivity of polymers at very low concentrations.[19] In addition, the graphene oxide geometry with its 2D structure and high ratio has helped to modify the polymer matrix structure and facilitate the development of microcapacitors in the composites, resulting in high permittivity, smooth processing, and lightweight.[20,21] Fazil et al. (2019) reported that polyimide composited with graphene oxide can increase the permittivity of the material.[22] In a similar study, Feng et al. (2021) reported that graphene in

Received: May 20, 2022
Accepted: August 29, 2022
Published: September 7, 2022

polythiocarbonate could increase the permeability of the composite. Inversely, the presence of graphene in polythiocarbonate decreased its dielectric loss.[23] Despite their outstanding performance when tested in their flexibility range, pure graphene or graphene oxide still shows limited buckling ability when subjected to narrow curvature or high mechanical deformation.[24,25]

Nanofiber composites can be used as a flexible candidate material for applications as electrode capacitors. Graphene oxide can be loaded into the nanofiber composites. The study of Sha et al. (2022) has succeeded in fabricating a flexible PVDF-co-hexafluoropropylene (PVDF-HFP) nanofiber membrane using the electrospinning method.[26] Another study has also reported that nanofiber membranes of lignin have been successfully fabricated with a diameter of 539 nm for flexible supercapacitors using polyacrylonitrile (PAN) also using the electrospinning method.[27] Edikresnha et al. (2019) have also successfully loaded glycerin and garlic extract into the PVP/CA nanofiber with a similar electrospinning method. The developed nanofiber had an average diameter of 797 nm, good mechanical strength, and was flexible enough for wound dressing applications.[28] The electrospinning technique is simple, adaptable, cost-efficient, and versatile. Additionally, it is easy to control the diameter, composition, morphology, and the flexibility of the produced nanofibers or membranes. The electrospun nanofibers feature many superior characteristics, such as high surface area to volume ratio and superior thermal and mechanical properties.[29] Due to these superior properties, nanofibers have been widely applied in biotechnology,[30] biomedical,[31,32] tissue engineering,[33] drug delivery,[34−36] filters for fluids,[37] and energy storage[38] applications. In addition, the electrospinning method also allows the production of nanofibers from various polymers.[39−41]

The choice of polymer or blend of polymers affects the formation of nanofiber membranes as well as their performance and flexibility. Some commonly used polymers are poly(3,4-ethylenedioxythiophene) (PEDOT),[42] polypropylene (PP),[43] polypyrrole (PPy),[44] and PAN.[45] PAN is an electrically conductive polymer studied intensively as a binder for electrode capacitors or supercapacitors. PAN also offers several favorable features, including easy integration, high flexibility, and conductivity (ferroelectricity and piezoelectricity).[46] These features allow PAN to form long-linked imine chains through polymerization of nitrile groups.[47] Another advantage is its broad use as a composite matrix in the manufacture of nanofiber membranes for its easy chemical interaction either as a pure polymer filler or other copolymer materials.[45] PAN is also widely found for various applications such as for biosensors, textiles, and corrosion protection.[48] The performance of graphene oxide from graphite can be increased by incorporating it into PAN nanofiber composites. The synergistic effect of carbon-based materials and conductive polymers in nanofiber composites has recently been shown to intensify the permeability of nanofiber membranes and reduce electric loss and flexibility.[49] Therefore, graphene oxide nanofiber composites from graphite and PAN are promising materials to improve dielectric properties and flexibility. In this research, graphene oxide/PAN composite fibers were produced with varying graphene oxide content. The flexible, morphology, and physicochemical properties were then investigated. Dielectric properties were also analyzed.

2. RESEARCH METHOD

2.1. Preparation of Materials. PAN (MW 1,50,000 kg mol^{-1}) and *N*,*N*-dimethylformamide (DMF, assay 99.0% min) were, respectively, purchased from Sigma-Aldrich (Singapore) and Merck (USA). Meanwhile, graphite (Powder 99.9%), distilled water, HCl (6 N), urea, iron (III) chloride ($FeCl_3$), and N_2 gas were obtained from Bratachem (Indonesia). All reagents were of analytical grade and used as received without further purification.

2.2. Preparation of Graphene Oxide and Synthesis of Nanofiber Membrane. Graphene oxide was synthesized from graphite. The method and procedure of producing graphene oxide were identical with the method and procedure of producing graphene oxide from palm kernel shells.[8] Furthermore, to create nanofiber membranes using the electrospinning method, the precursor solution was made by dissolving PAN 10% w/w into DMF solvent and graphene oxide from graphite. The weight of the graphene oxide dissolved varied, such as 0.04, 0.14, and 0.24 g, respectively. Each precursor solution to produce nanofibers, as given in Table 1, was labeled as GN1, GN2, and GN3. In order to achieve a homogeneous and black solution, each material was mixed on a hotplate-magnetic stirring (Therumo Sci., Japan) at a temperature of 80 °C and at a constant speed of 200 rpm for 24 h. The electrospinning apparatus (Nanolab ES/DS 106, Malaysia) was used to synthesize nanofibers from the precursor solutions. The precursor solutions (GN1, GN2, and GN3) were transferred into a 10 mL syringe (Terumo, Japan) equipped with a 21-gauge needle with 0.80 mm inner diameter. The solution was dispensed with a syringe pump at a constant flow rate of 4 mL per hour. The parameters of the electrospinning were 12 kV high voltage, 8 cm gap distance of 20 cm, and 300 rpm of fiber rotation. The temperature and humidity of the controlled chambers were kept at 25 °C and 40−50%, respectively.

Table 1. Mass of PAN and Graphene Oxide for the Electrospinning Process

precursor solution	PAN (w/w)	GO (g)
GN1	10%	0.04
GN2	10%	0.14
GN3	10%	0.24

2.3. Characterization. The graphene oxide morphology was observed using a transmission electron microscope (HT7700, USA), and the morphology of graphene oxide was investigated using scanning electron microscopy (SEM) (Vega 3 Tescan, Japan) with the excitation voltage of 10 kV and an optical magnification of 10,000 times. The results were declared in mean ± standard deviation (SD). Statistical differences between groups were analyzed using one-way ANOVA followed by Tukey's HSD (honestly significant difference) post hoc test.[56] This statistical test employed IBM SPSS 20 software (IBM, USA) to determine a significant difference with the confidence level higher than 95% ($p < 0.05$).[56] The presence of functional groups and intermolecular interaction were identified by using a Fourier transform infrared (FTIR) spectroscope (Thermo Nicolet iS10, Japan). The crystal structure of composite nanofibers was recorded using X-ray diffraction (XRD) (Rigaku MiniFlex 600, Japan). Tensile strength and Young's modulus of all the nanofibrous mats were investigated by the grab and strip method using a

https://doi.org/10.1021/acsomega.2c03144
ACS Omega 2022, 7, 33087−33096

FAVIGRAPH tensile tester (Textechno H. Stein GmbH & Co, Germany). Samples 3−20 mm in size with the same thickness were clamped on both sides of the tool and then were pulled at a speed of 20 mm per minute. Furthermore, the load cell was 100 cN and the gauge length was 10 mm. The level of extension and the length of measurement were identical to the previous experiment.[50] The maximum tensile strength (UTS) was indicated by the highest stress point on the curve, whereas Young's modulus was calculated from the ratio of the stress over strain for the linear portion of the curve. The dielectric properties were analyzed using dielectric spectroscopy (Hioki 3532-50 LCR HiTester, Japan). The diameter of the nanofiber sample was about 8 × 8 × 4 mm which was placed between two parallel electrodes. The measurements were conducted at room temperature, voltage amplitude 1.4 V, and frequency range of 50−500 kHz.

3. RESULTS AND DISCUSSION

3.1. Morphology of GO and Nanofiber Mats. Graphene oxide (GO) from graphite was formed through the pyrolysis process. The formation was mainly due to the effect of temperature increase from 700 to 900 °C. This result is the same as our previous study report.[8] The morphology of graphene oxide from graphite is shown from SEM and transmission electron microscopy (TEM) results in Figure 1a,b. The wavy morphology of GO is caused by the bending of

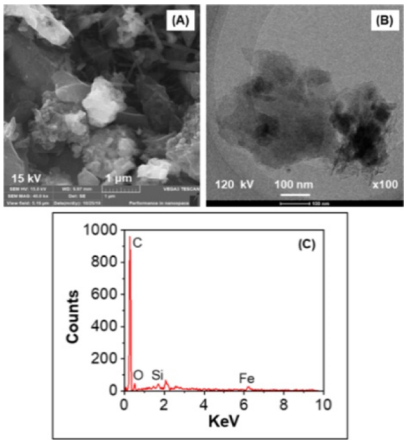

Figure 1. (a) SEM, (b) TEM, and (c) EDX of graphene oxide from graphite.

the 2D sheet, which results in a more thermodynamically stable tangled structure.[8,51] In addition, the buildup of GO was reduced due to the exfoliation of the graphite structure. The oxidant-reduction of graphene is in line with the data of the EDX spectrum shown in Figure 1c. As expected, the oxygen peak in graphene oxide was only 6.96% and carbon peak was 87.8%.

Figure 2a displays the PAN and PAN solutions with different graphene oxide contents. The three neat solutions are black in color and homogeneous. They do not clog on the tip of the nozzle, although they have high viscosity and fast solvent evaporation. Figure 2b exhibits the pure PAN membrane and the GN1, GN2, and GN3 nanofiber composites. The membranes have a smooth surface and are black in color, which corresponds to the color of the solution prior to the electrospinning process. Nanofiber membranes can be bent to a radius of 1 cm (Figure 2c,d), indicating the flexibility of the

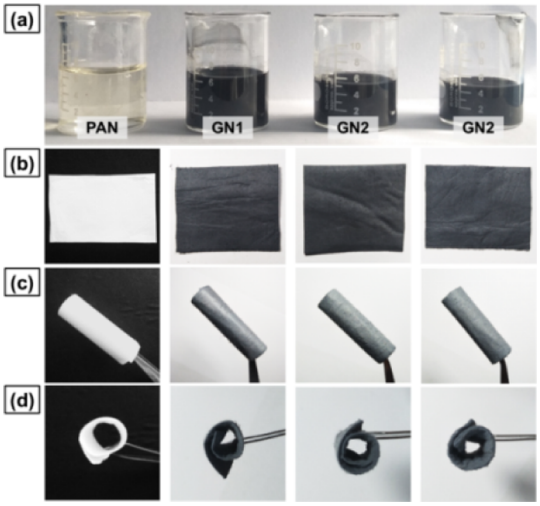

Figure 2. (a) Pure PAN solution and PAN solution containing graphene oxide, (b) pure PAN membrane and GN1, GN2, and GN3 nanofiber composites, membranes with (c) longitudinal and (d) transverse positions. Photograph courtesy of Muhammad Rama Almafie. Copyright 2022.

membrane and it is explained in more detail in mechanical analysis. The obtained nanofibers were stored in a dry cabinet with a temperature of 30° and a relative humidity of 50%.

3.2. SEM Micrographs. The morphology of the electrospun fibers is usually in the form of fine fiber, bead fiber, and simple fiber. In this study, the morphology of the fibers was investigated from three different precursor solutions. The three PAN fibers loaded with graphene oxide had a uniform shape and were free of beads as shown from the SEM results in Figure 3. The uniform fiber morphology formation indicated sufficient polymer concentration in the precursor for the electrospinning process. At a concentration of 10% w/w a PAN with a molecular weight of 1,50,000 kg mol^{-1} can produce a perfect membrane without fiber beads.[52] While Samadian et al. (2017) in their study reported that PAN with a molecular

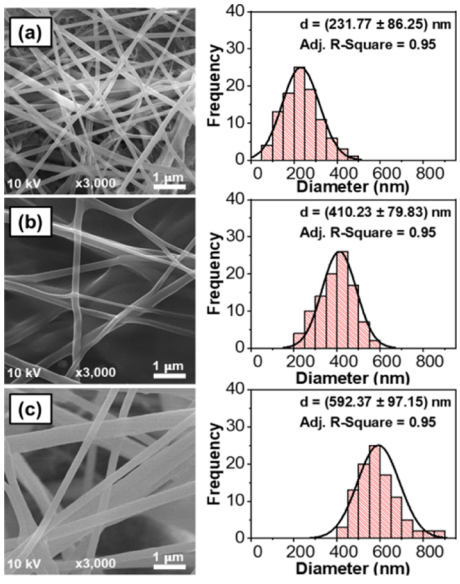

Figure 3. Morphology and diameter distributions of the nanofibrous electrode: (a) GN1, (b) GN2, and (c) GN3.

https://doi.org/10.1021/acsomega.2c03144
ACS Omega 2022, 7, 33087−33096

weight of 80,000 kg mol^{-1} (7% w/w) produced a membrane with beaded fiber.[53] The polymer concentration is important to form a continuous and homogeneous nanofiber membrane.

The homogeneity of GN1, GN2, and GN3 fibers was also investigated using the coefficient of variation (CV) of the fibers. A membrane with homogeneous fibers has a CV of less than 0.3, with a lower CV, indicating a greater degree of homogeneity.[54] Fibers of GN2 and GN3 with CV values of 0.19 and 0.16, respectively, were more uniform than GN1 with a CV value of 0.37. The lower fiber homogeneity may be due to current fluctuations during the electrospinning process as a control measure system to maintain a constant current is not applied to this electrospinning system. Another factor that might contribute to the lower homogeneity is the use of a high voltage of 12 kV. High voltages can cause an imbalance between precursor loading and load-induced spinning.[55] As a result, one or more side jets are formed to produce fibers of inconsistent size. From the statistical analysis, there was significant ($p < 0.05$) between GN1 and GN2, and there was significant ($p < 0.05$) between GN1 and GN3. On the other hand, there was significant ($p < 0.05$) between GN2 and GN3.

The effect of the difference in the graphene concentration in PAN on the fiber diameter is shown in Figure 3. GN3 fiber with a higher mass of graphene produces a larger diameter of 592.37 nm. Correspondingly, lowering the concentration can decrease the fiber diameter. As in the diameter of GN2 and GN1 fibers, they decreased to 410.27 and 231.77 nm, respectively. The fiber diameter is tightly controlled by the viscosity of the solution, wherein the degree of chain bonding decreases with lower viscosity, leading to the formation of smaller diameters. The addition of graphene oxide in the PAN nanofiber did not change the shape of the fiber, but it did affect the diameter of the fiber. This is in line with results of a previous study that the addition of graphene in polyethylene terephthalate increases the fiber diameter.[56]

3.3. Mechanical Properties. In electronic equipment, the mechanical properties of dielectric materials play an important role for practical and flexible applications. The investigation of the mechanical properties was conducted to determine the flexible properties of composite nanofiber mats. A set of curves provides the relationship between stress and strain for all nanofibers in which the mean strain at break, ultimate tensile strength, and Young's modulus are shown in Figure 4. Pure PAN exhibits ultimate tensile strength, strain at break, and Young's modulus of 2.16 MPa, 9.19%, and 23.50 MPa, respectively. When PAN and GO are fabricated into composites, the tensile strength of the nanofiber composite mats ranged from 3.9 to 8.8 MPa, which exceeded that of typical CNFs (~0.48 MPa). This is higher than PAN at a concentration of 14%, and the previously studied carbon nanofibers.[52,57] These results indicated that the flexible nanofiber mat electrodes could serve as capacitor electrodes.

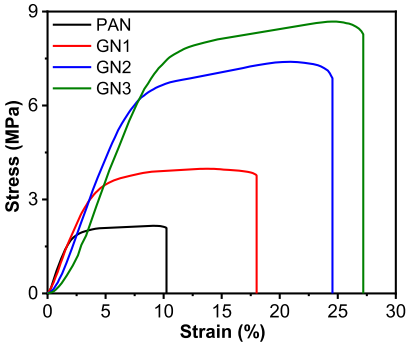

Figure 4. Relation between stress and strain for all the fibrous mats.

3.4. FTIR Spectroscopy. The chemical structures of PAN, GO, PAN/GO GN1, GN2, and GN3 nanofiber composites were observed by the FTIR spectrum (Figure 5). The

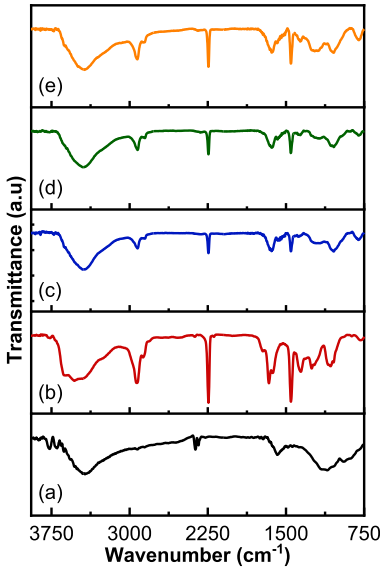

Figure 5. FTIR measurements for (a) GO, (b) PAN, (c) GN1, (d) GN2, and (e) GN3.

characteristic peak of the GO functional group emerged at 3427, 2370, 1716, 1581, and 1103 cm^{-1}. The peak at 3427 cm^{-1} indicated O−H stretching. This peak confirms that the emerging hydroxyl peak may be due to the absorption of water vapor on the GO surface.[8,58,59] The peak at 2370 cm^{-1} was O═C═O stretching, indicating a carbon dioxide group.[60] The emergence of the carbon peak was in line with the EDX analysis. The peak of moderate intensity at 1716 cm^{-1} indicated the C═O stretching of carboxylic acid.[61−63] The peak at 1579 cm^{-1} is a symmetrical C═C stretching vibration of the aromatic group, and the peak at 1103 cm^{-1} can be attributed to the C−C asymmetric stretching vibration of the aromatic group.[61,64] In addition, the two shoulder peaks at 2848 and 2927 cm^{-1} corresponded to the C−H aromatic sp^2 strain vibrations.[65,66] In the FTIR GO spectrum, the hydroxyl and carboxyl peaks have indicated oxidation.[67,68] The insertion of functional oxygen-carrying groups in the GO form exhibited that the acidic and oxidative compounds successfully modified the surface, and this is in line with the SEM and TEM results.

The PAN FITR spectrum displayed typical broad peaks at 3531, 2927, 2243, 1724, 1664, 1452, 1357, 1251, and 1,076 cm^{-1}. The wide peak of hydroxyl at 3531 cm^{-1} corresponds to stretching vibrations of −OH.[69,70] The peak of 2243 cm-^{1} is the stretching vibration of C≡N. The peaks of 2931, 1452, and 1327−1392 cm^{-1} were designated as bending and stretching vibrations of CH_2, and the weak intensity peaks at 1724 cm^{-1} represented the stretching vibration of CO.[57,71,72] The functional ester groups at 1230−1250 and 1050−1090 cm^{-1} were defined as strain vibrations of C−O and C−O−C. These results indicate that PAN is a copolymer of acrylonitrile and methyl acrylate such as itaconic acid or methyl acrylate which is frequently used in the industrial production of

https://doi.org/10.1021/acsomega.2c03144
ACS Omega 2022, 7, 33087−33096

PAN.[73,74] The peak at 1,665 cm^{-1} was assigned to the C═N bond strain vibration of the middle oxime group.[75,76] The peaks of this PAN will decrease and increase due to the concentration of PAN when composites involve other materials such as carbon[71] and conductive polymers.[77]

The addition of GO to the PAN nanofibers caused changes in the intensity and positions of some peaks in the spectra of the GN1, GN2, and GN3 samples. The stretch peaks of GN1, GN2, and GN3 composite nanofiber mats were at 3434, 3452, and 3461 cm^{-1}, respectively, which was higher than GO at 3427 cm^{-1}. The peak of the nitrile group shifted to below 2243 cm^{-1} in the spectrum of 2242 cm^{-1} (GN1), 2244 cm^{-1} (GN2), and 2242 cm^{-1} (GN3). This peak decreased in intensity when the C≡N group was introduced to PAN-grafted GO surfaces. The 1634 cm^{-1} (GN1), 1639 cm^{-1} (GN2), and 1642 cm^{-1} (GN3) peaks were lower than that of the PAN at 1665 cm^{-1}. The shift of the peaks in the composite nanofiber mats is due to the interaction between PAN and GO molecules through hydrogen bonds.

3.5. X-ray Diffraction Spectra Analysis. XRD is widely used to understand the structural modifications in polymer blends which depend on the complexation of the carbon material. The complexation is done by analyzing the position, shift, and expansion of the diffraction peaks in the XRD pattern of each polymer sample. Figure 6 shows the diffraction spectra

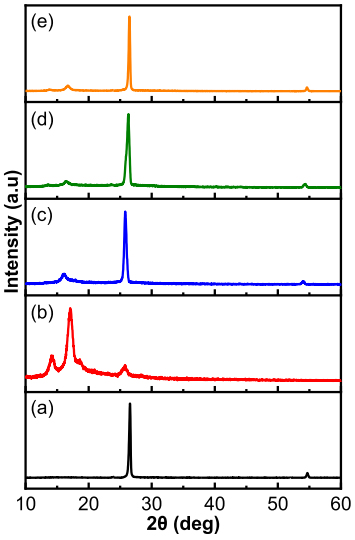

Figure 6. XRD spectra for (a) GO, (b) PAN, (c) GN1, (d) GN2, and (e) GN3.

of GO, PAN, composite PAN/GO for GN1, GN2, and GN3. The most obvious diffraction pattern displays two characteristic peaks of graphite-based GO crystal properties at 2θ positions of 25.65 and 54.68°, both of which correspond to the crystal planes (0 0 2)[78,79] and (0 0 4),[79] this implies that GO is pure crystalline.[78,80] The diffraction pattern of the PAN nanofiber membrane has characteristic peaks at 14 and 17° corresponding to the (0 2 0) and (0 1 0) planes.[8,81,82] These two peaks indicate that PAN is a crystalline structure.

The addition of GO to PAN nanofibers resulted in a new characteristic peak diffraction pattern from the pure PAN XRD pattern. Very sharp peaks occurred between 20 and 30°, that is, 25, 25.36, and 26.46° were associated with successful GO grafting on the PAN polymer backbone of the GN1, GN2, and GN3 composites, respectively. The characteristic PAN peak has only one diffraction pattern with relatively weak peak intensity observed at 15° (GN1), 15.32° (GN2), and 16.66° (GN3). This shows that GO nanofibers are well distributed in the PAN matrix, and this filler does not affect the crystal structure, it only changes the connection between the two phases (PAN and GO) and improves interfacial compatibility. The results from previous studies revealed that the addition of carbon nanotubes in polyurethane did not affect the structure of the composite crystals.[83]

XRD data of all PAN/GO nanofiber composites were analyzed using OriginPro 9 (OriginLab Corp.) to calculate the percentage variation of crystallinity in the composite fibers as the function of GO concentration.[84] The addition of GO increased the percentage of crystallinity of GN1, GN2, and GN3 to 85.52, 86.12, and 86.23%, respectively. This is because GO can associate with the PAN functional group so as to support the process of increasing the crystal phase content in the nanofiber mat composite.

3.6. DSC Analysis. Differential scanning calorimetry (DSC) thermographs of PAN, GO, GN1, GN2, and GN3 nanofiber composites are shown in Figure 7. The PAN showed

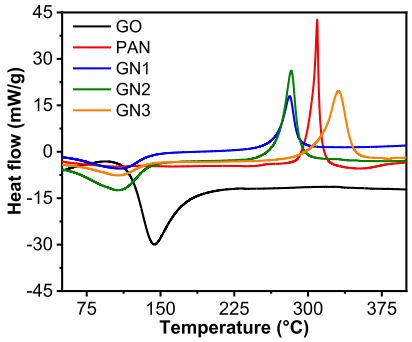

Figure 7. Differential scanning calorimetry analysis.

an exothermic crystallization transition at 192°, which represents the melting temperature of PAN. Furthermore, the DSC thermogram of GO displayed an endothermic melting transition at 178°. After the addition of the GO material to the PAN matrix, all composite samples showed relatively sharp melting peaks and relatively broad crystal peaks, which allowed melting or recrystallization. Because this occurs during heating, the value of enthalpy (ΔH) from the integration of endothermic and exothermic can be visualized and compared with the fusion crystalline domain progressively created during the previous isothermal period.[84] The increase in melting temperature (Tm) is relatively shifted toward a higher temperature and the crystal temperature (Tc) shifts toward a lower temperature, that is, Tm: 281.28, 282.92, and 330.97 °C and Tc: 108.84, 106.94, and 106.74 °C of the GN1, GN2, and GN3 composites, respectively. Meanwhile, the values of enthalpy of fusion (ΔHm) were 110.69 J/g (GN1), 165.08 J/g (GN2), and 204.92 J/g (GN3), and the values of enthalpy of melting (ΔHc) were 85.58 J/g (GN1), 129.11 J/g (GN2), and 68.03 J/g (GN3).

The change in value specifically indicated that the GO sheet acted as a nucleating agent that increases the thermal stability of the composite.[85] In addition, the increase in Tm and Tc due to intermolecular interactions as well as the increase in the degree of crystallization is in line with the XRD and FTIR results. The increase in hydrogen bonds between PAN and GO molecules freed the movement of polymer molecular chains

https://doi.org/10.1021/acsomega.2c03144
ACS Omega 2022, 7, 33087−33096

which results in an increase in the degree of crystallinity of the composite.[59,86] The PAN molecular chain becomes disorganized because the PAN structure disintegrated with the increase in GO content and consequently strengthened the contact between PAN and GO.[29,87] At the same time, more ester groups were hydrolyzed followed by an increase in the hydroxyl number. This resulted in more intermolecular hydrogen bonding which in turn improved the thermal properties.[86,88]

3.7. Dielectric Properties. The relative permittivity and dielectric loss are important factors in determining the electric field distribution and heat production in the dielectric with an alternating current electric field. Because different types of polarization will dominate the entire dielectric polarization at different frequencies, these two parameters are highly dependent on the frequency of the external electric field.[89,90] The frequency dependence (relative permittivity component), as determined at an ambient temperature of 50 to 10^6 Hz, of the PAN/GO composite is shown in Figure 8a. At low frequencies,

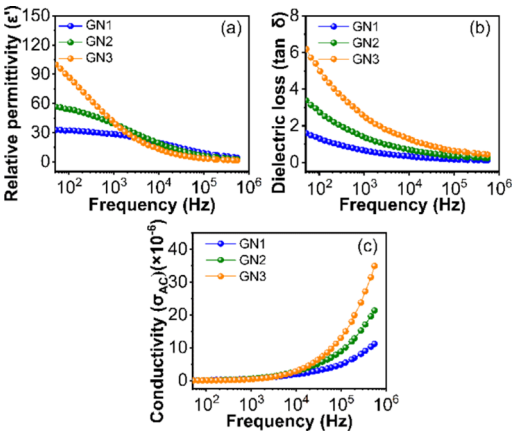

Figure 8. (a) Relative permittivity (ε'), (b) dielectric loss (tan δ), and (c) electrical AC conductivity (σ_{AC}) of PAN/GO of GN1, GN2, and GN3.

the relative permittivity of all samples was significantly higher than at high frequencies. This is because the interface and orientation polarization dominate the total polarization. In addition, electron polarization dominated at high frequencies.[90,91] The permittivity was relatively high at lower frequencies (below 1000 Hz). This is because both induced and permanent dipoles can accommodate themselves to line up in a proper orientation alignment in this region, a phenomenon known as the Maxwell Wagner Sillar effect (MWS).[92,93] Furthermore, this finding indicates that the low-frequency electrical field allows more time for the dipole moment to reach polarization equilibrium.[94] The relative permittivity generally remained stable at high frequencies (more than 1,00,000 Hz) because it was frequency-independent. This feature is known as the microcapacitor structure model.[92] The electric field changes so dramatically that the carriers cannot align, and as a result, they cannot reach the grain boundaries and there is no polarization.[91,95]

The relative permittivity increased when the mass of the GO fraction was increased from 32.2 (GN1) to 86.4 (GN3) at a frequency of 10^2 Hz. This is because GO is conductive, resulting in an increase in interfacial polarization which can lead to an increase in the relative permittivity of the nanofiber mat composite. The addition of GO has also caused a large amount of free charge to accumulate at the component interface, resulting in the formation of additional dipoles.[11,92] In addition, the nanostructures described in the SEM analysis generally have a high surface area, thus providing a larger amount of space to store the charge.

The dielectric loss (tan δ) of the PAN/GO composite is shown in Figure 8b. The dielectric losses reached their maximum values of 1.59, 3.39, and 6.18, at 50 Hz, respectively, of GN1, GN2, and GN3. Increasing the frequency lowers the dielectric loss. At 1000−1,00,000 Hz, the decrease becomes frequency-dependent, with the dielectric samples GN1, GN2, and GN3 decreasing from 0.63, 1.32, and 2.42 to 0.16, 0.34, and 0.63. At frequencies above 5,00,000 Hz, the dielectric loss no longer depends on the frequency so that it reaches a value below the minimum. This was because the charge carriers can follow the rapidly changing electric field. Due to the phenomenon of space charge polarization, which is responsible for the Shockley process, dielectric losses at low frequencies were quite low in this situation.[95,96] Dielectric loss was shown to be dependent on the PAN/GO of GN1, GN2, and GN3 composites at high frequencies, which can be explained by Maxwell Wagner relaxation.[94] A large number of oxygen-enriched groups formed the GO surface sheet. This oxygen-rich group was resistive and created a lot of polarization, which means it has a lower dielectric loss.[95] Consequently, adding GO in the PAN matrix lowered the dielectric loss. The internal polarization relaxation of the interface caused a decrease in the dielectric loss. This is because the polarization of the space charge can follow the electric field. As a result, the relaxation caused a decrease in the dielectric loss, and the addition of GO inhibited the movement of electrons in the polymer chain.[97] With its high aspect ratio and 2-dimensional structure, GO provides more interfacial area in the polymer matrix, resulting in decreased interfacial polarization and space charge polarization.

Figure 8c shows the conductivity frequencies of PAN/GO GN1, GN2, and GN3. At low frequencies (below 1000 Hz), the conductivity of all samples was independent of the frequency. The externally applied electric field has insufficient energy in this range to allow charge flow in a non-unidirectional way. Therefore, charge carriers were randomly oriented at these frequencies.[94,95,98] As the energy of some of the charge carriers grew at the intermediate frequency level, they began to flow toward the field. Due to the much larger external field, this process of moving charge carriers was accelerated exponentially at much higher frequencies. In the frequency range above 10,000−5,00,000 Hz, the composite conductivity increased gradually from 1.6×10^{-6} Sm^{-1} to 34.9×10^{-6} Sm^{-1}. Through loop mechanics, this flow increased exponentially at much higher frequencies. The increase in the surface area and the density of defects of the nanofiber composites led to the trapping of a large amount of charges. This caused the high-frequency state that allowed the charge to be released and yield an increase in the combined conductivity.[8,11] As a result, each sample has satisfied the requirements of the dielectric characteristics, that is, relative permittivity values, dielectric loss, and conductivity.

4. CONCLUSIONS

Composite materials with PAN as polymer and graphene oxide (GO) derived from graphite was successfully developed. It was synthesized using the electrospinning method to form PAN/GO nanofiber composites. It was observed that the electrospun

https://doi.org/10.1021/acsomega.2c03144
ACS Omega 2022, 7, 33087−33096

PAN/GO nanofiber composites were produced homogeneously, and flexible composite fiber mats with maximum tensile strengths of 2.48−8.67 MPa, strains of 13.84, 20.93, and 24.88%, and the Young's modulus continued to decrease with the increase in GO content. FTIR and XRD recordings showed that GO interactions were dominant over PAN, indicating that GO was evenly distributed in the PAN matrix. This was indicated by the strengthening behavior at the sharp peak of crystallization with a maximum degree of crystallinity of 86.23%. Other indications also included stronger hydrogen bonds and more hydrolyzed ester groups. This fact was supported by the increase in enthalpy from 110.69 to 204.92 J/g. It has been determined that the true part of the dielectric properties displays a dependent behavior at a frequency of approximately 50 Hz to 10,00,000 Hz regardless of the GO filler presentation. The relative permittivity increased from 32.2 (0.08 w/w) (GN1) to 86.4 (0.24 w/w) (GN3) at a frequency of 10^2 Hz. Maximum conductivity has been achieved at a value of 34.9×10^{-6} Sm^{-1} at high frequencies. Therefore, we hope that this work paves the way for optimal solutions in preparing PAN/GO composite materials that ensure superior properties for energy storage applications.

AUTHOR INFORMATION

Corresponding Author

Ida Sriyanti − *Physics Education, Universitas Sriwijaya, Indralaya 30662, Indonesia; Laboratory of Instrumentation and Nanotechnology Applications, Universitas Sriwijaya, Indralaya 30662, Indonesia;* orcid.org/0000-0001-8011-8866; Email: ida_sriyanti@unsri.ac.id

Authors

Muhammad Rama Almafie − *Physics Education, Universitas Sriwijaya, Indralaya 30662, Indonesia; Laboratory of Instrumentation and Nanotechnology Applications, Universitas Sriwijaya, Indralaya 30662, Indonesia*

Leni Marlina − *Physics Education, Universitas Sriwijaya, Indralaya 30662, Indonesia*

Riyanto Riyanto − *Biology Education, Universitas Sriwijaya, Indralaya 30662, Indonesia*

Jaidan Jauhari − *Department of Computer Science and Laboratory of Instrumentation and Nanotechnology Applications, Universitas Sriwijaya, Indralaya 30662, Indonesia*

Zainuddin Nawawi − *Department of Electrical Engineering, Universitas Sriwijaya, Indralaya 30662, Indonesia*

Complete contact information is available at: https://pubs.acs.org/10.1021/acsomega.2c03144

Author Contributions

M.R.A. contributed to conceptualization, methodology, software, carried out data curation, and writing of original draft. J.J. performed investigation and formal analysis. L.M. contributed to supervision. R.R. contributed to formal analysis. Z.N. contributed to supervision. I.S. contributed to supervision, funding acquisition, and writing—review and editing.

Notes

The authors declare no competing financial interest.

ACKNOWLEDGMENTS

This research of this article was funded by DIPA of Public Service Agency of Universitas Sriwijaya 2022. SP DIPA-023.17.2.677515/2022, on December 13, 2021 (The additional output of research).

REFERENCES

(1) Do, T. C.; Truong, H. V. A.; Dao, H. V.; Ho, C. M.; To, X. D.; Dang, T. D.; Ahn, K. K. Energy Management Strategy of a PEM Fuel Cell Excavator with a Supercapacitor/Battery Hybrid Power Source. *Energies* **2019**, *12*, 4362.

(2) Vera, Y. E. G.; Dufo-López, R.; Bernal-Agustín, J. L. Energy Management in Microgrids with Renewable Energy Sources: A Literature Review. *Appl. Sci.* **2019**, *9*, 3854.

(3) Zhu, J.; Roscow, J.; Chandrasekaran, S.; Deng, L.; Zhang, P.; He, T.; Wang, K.; Huang, L. Biomass-Derived Carbons for Sodium-Ion Batteries and Sodium-Ion Capacitors. *ChemSusChem* **2020**, *13*, 1275−1295.

(4) Kumar, A.; Bhattacharya, T.; Mozammil Hasnain, S. M.; Kumar Nayak, A.; Hasnain, M. S. Applications of Biomass-Derived Materials for Energy Production, Conversion, and Storage. *Mater. Sci. Energy Technol.* **2020**, *3*, 905−920.

(5) Wang, Z.; Carriveau, R.; Ting, D. S. K.; Xiong, W.; Wang, Z. A Review of Marine Renewable Energy Storage. *Int. J. Energy Res.* **2019**, *43*, 6108−6150.

(6) Luta, D. N.; Raji, A. K. Optimal Sizing of Hybrid Fuel Cell-Supercapacitor Storage System for off-Grid Renewable Applications. *Energy* **2019**, *166*, 530−540.

(7) Phiri, J.; Dou, J.; Vuorinen, T.; Gane, P. A. C.; Maloney, T. C. Highly Porous Willow Wood-Derived Activated Carbon for High-Performance Supercapacitor Electrodes. *ACS Omega* **2019**, *4*, 18108−18117.

(8) Jauhari, J.; Almafie, M. R.; Marlina, L.; Nawawi, Z.; Sriyanti, I. Physicochemical Properties and Performance of Graphene Oxide/Polyacrylonitrile Composite Fibers as Supercapacitor Electrode Materials. *RSC Adv.* **2021**, *11*, 11233−11243.

(9) Bagarti, T.; Jayannavar, A. M. Storage of Electrical Energy: Batteries and Supercapacitors. *Resonance* **2020**, *25*, 963−980.

(10) Pawar, S. P.; Arjmand, M.; Pötschke, P.; Krause, B.; Fischer, D.; Bose, S.; Sundararaj, U. Tuneable Dielectric Properties Derived from Nitrogen-Doped Carbon Nanotubes in PVDF-Based Nanocomposites. *ACS Omega* **2018**, *3*, 9966−9980.

(11) Ishaq, S.; Kanwal, F.; Atiq, S.; Moussa, M.; Azhar, U.; Gul, I.; Losic, D. Dielectric and Impedance Spectroscopic Studies of Three Phase Graphene/Titania/Poly(Vinyl Alcohol) Nanocomposite Films. *Results Phys.* **2018**, *11*, 540−548.

(12) Chen, M.; Zhou, W.; Zhang, J.; Chen, Q. Dielectric Property and Space Charge Behavior of Polyimide/Silicon Nitride Nanocomposite Films. *Polymers* **2020**, *12*, 1−12.

(13) Zhao, M.; Fu, Q.; Hou, Y.; Luo, L.; Li, W. BaTiO3/MWNTs/Polyvinylidene Fluoride Ternary Dielectric Composites with Excellent Dielectric Property, High Breakdown Strength, and High-Energy Storage Density. *ACS Omega* **2019**, *4*, 1000−1006.

(14) Volosova, M. A.; Okunkova, A. A.; Fedorov, S. V.; Hamdy, K.; Mikhailova, M. A. Electrical Discharge Machining Non-Conductive Ceramics: Combination of Materials. *Technologies* **2020**, *8*, 32.

(15) Oba, F.; Kumagai, Y. Design and Exploration of Semiconductors from First Principles: A Review of Recent Advances. *Appl. Phys. Express* **2018**, *11*, 060101.

(16) Wang, J.; Xue, M.; Liu, H.; Yuan, M.; Bai, D.; Tang, G.; Zhang, J.; Stampfl, C. Stability and Band Offsets between GaAs Semiconductor and CeO 2 Gate Dielectric. *AIP Adv.* **2019**, *9*, 025117.

(17) Li, M.; Mu, B. Effect of Different Dimensional Carbon Materials on the Properties and Application of Phase Change Materials: A Review. *Appl. Energy* **2019**, *242*, 695−715.

(18) Wang, Y.; He, P.; Li, F. Graphene-Improved Dielectric Property of CCTO/PVDF Composite Film. *Ferroelectrics* **2019**, *540*, 154−161.

(19) Bayer, T.; Bishop, S. R.; Perry, N. H.; Sasaki, K.; Lyth, S. M. Tunable Mixed Ionic/Electronic Conductivity and Permittivity of Graphene Oxide Paper for Electrochemical Energy Conversion. *ACS Appl. Mater. Interfaces* **2016**, *8*, 11466−11475.

(20) Andre, R. S.; Mercante, L. A.; Facure, M. H. M.; Mattoso, L. H. C.; Correa, D. S. Enhanced and Selective Ammonia Detection Using In 2 O 3 /Reduced Graphene Oxide Hybrid Nanofibers. *Appl. Surf. Sci.* **2019**, *473*, 133−140.
(21) He, G.; Song, Y.; Chen, S.; Wang, L. Porous Carbon Nanofiber Mats from Electrospun Polyacrylonitrile/Polymethylmethacrylate Composite Nanofibers for Supercapacitor Electrode Materials. *J. Mater. Sci.* **2018**, *53*, 9721−9730.
(22) Fazil, S.; Bangesh, M.; Rehman, W.; Liaqat, K.; Saeed, S.; Sajid, M.; Waseem, M.; Shakeel, M.; Bibi, I.; Guo, C. Y. Mechanical, Thermal, and Dielectric Properties of Functionalized Graphene Oxide/Polyimide Nanocomposite Films. *Nanomater. Nanotechnol.* **2019**, *9*, 1−8.
(23) Feng, Z.; Zhang, X. H. Highly Stretchable Poly-(Thiocarbonate)/Graphene Oxide Dielectric Composites toward a High Dielectric Constant and Low Dielectric Loss. *ACS Appl. Polym. Mater.* **2021**, *3*, 3586−3594.
(24) Ahmed, R. M.; Ibrahiem, A. A.; El-Bayoumi, A. S.; Atta, M. M. Structural, Mechanical, and Dielectric Properties of Polyvinylchloride/Graphene Nano Platelets Composites. *Int. J. Polym. Anal. Charact.* **2021**, *26*, 68−83.
(25) Zhou, L.; Qiu, J.; Wang, X.; Wang, H.; Wang, Z.; Fang, D.; Li, Z. Mechanical and Dielectric Properties of Reduced Graphene Oxide Nanosheets/Alumina Composite Ceramics. *Ceram. Int.* **2020**, *46*, 19731−19737.
(26) Sha, Z.; Boyer, C.; Li, G.; Yu, Y.; Allioux, F. M.; Kalantar-Zadeh, K.; Wang, C. H.; Zhang, J. Electrospun Liquid Metal/PVDF-HFP Nanofiber Membranes with Exceptional Triboelectric Performance. *Nano Energy* **2022**, *92*, 106713.
(27) Wu, H.; Liu, C.; Jiang, Z.; Yang, Z.; Mao, X.; Wei, L.; Sun, R. Electrospun Flexible Lignin/Polyacrylonitrile-Based Carbon Nanofiber and Its Application in Electrode Materials for Supercapacitors. *Text. Res. J.* **2022**, *92*, 456−466.
(28) Edikresnha, D.; Suciati, T.; Munir, M. M.; Khairurrijal, K. Polyvinylpyrrolidone/Cellulose Acetate Electrospun Composite Nanofibres Loaded by Glycerine and Garlic Extract with: In Vitro Antibacterial Activity and Release Behaviour Test. *RSC Adv.* **2019**, *9*, 26351−26363.
(29) Parameswaranpillai, J.; Elamon, R.; Sanjay, M. R.; Siengchin, S. Synergistic Effects of Ethylene Propylene Diene Copolymer and Carbon Nanofiber on the Thermo-Mechanical Properties of Polypropylene/High-Density Polyethylene Composites. *Mater. Res. Express* **2019**, *6*, 085302.
(30) Hashmi, M.; Ullah, S.; Kim, I. S. Copper Oxide (CuO) Loaded Polyacrylonitrile (PAN) Nanofiber Membranes for Antimicrobial Breath Mask Applications. *Curr. Res. Biotechnol.* **2019**, *1*, 1−10.
(31) Sriyanti, I.; Edikresnha, D.; Rahma, A.; Miftahul Munir, M. M.; Rachmawati, H.; Khairurrijal, K. Mangosteen Pericarp Extract Embedded in Electrospun PVP Nanofiber Mats: Physicochemical Properties and Release Mechanism of α-Mangostin. *Int. J. Nanomed.* **2018**, *13*, 4927−4941.
(32) Sriyanti, I.; Edikresnha, D.; Rahma, A.; Munir, M. M.; Rachmawati, H.; Khairurrijal, K. Correlation between Structures and Antioxidant Activities of Polyvinylpyrrolidone/Garcinia Mangostana L. Extract Composite Nanofiber Mats Prepared Using Electrospinnin. *J. Nanomater.* **2017**, *2017*, 1−10.
(33) Dwitiyanti D, D.; Harahap, Y.; Elya, B.; Bahtiar, A. Impact of Solvent on the Characteristics of Standardized Binahong Leaf (Anredera Cordifolia (Ten.) Steenis). *Pharmacogn. J.* **2019**, *11*, 1463−1470.
(34) Sriyanti, I.; Edikresnha, D.; Munir, M. M.; Rachmawati, H.; Khairurrijal. Electrospun Polyvinylpyrrolidone (PVP) Nanofiber Mats Loaded by Garcinia Mangostana L. Extracts. *Mater. Sci. Forum* **2017**, *880*, 11−14.
(35) Edikresnha, D.; Suciati, T.; Khairurrijal, K. Preliminary study of composite fibers polyvinylpyrrolidone/cellulose acetate loaded by garlic extract by means of electrospinning method. *Mater. Today: Proc.* **2021**, *44*, A1−A4.
(36) Andjani, D.; Sriyanti, I.; Fauzi, A.; Edikresnha, D.; Munir, M. M.; Rachmawati, H.; Khairurrijal, K. Rotary Forcespun Polyvinylpyrrolidone (PVP) Fibers as a Mangosteen Pericarp Extracts Carrier. *Procedia Eng.* **2017**, *170*, 14−18.
(37) Essa, W. K.; Yasin, S. A.; Saeed, I. A.; Ali, G. A. M. Nanofiber-Based Face Masks and Respirators as Covid-19 Protection: A Review. *Membranes* **2021**, *11*, 250.
(38) Kyeremateng, N. A.; Gukte, D.; Ferch, M.; Buk, J.; Hrebicek, T.; Hahn, R. Preparation of a Self-Supported SiO_2 Membrane as a Separator for Lithium-Ion Batteries. *Batteries Supercaps* **2020**, *3*, 456−462.
(39) Edikresnha, D.; Suciati, T.; Khairurrijal, K. Study of morphology of composite fibers polyvinylpyrrolidone/cellulose acetate loaded by garlic extract with glycerin as an additive. *Mater. Today: Proc.* **2021**, *44*, A5−A8.
(40) Kusumah, F. H.; Sriyanti, I.; Edikresnha, D.; Munir, M. M.; Khairurrijal. Simply Electrospun Gelatin/Cellulose Acetate Nanofibers and Their Physico-Chemical Characteristics. *Mater. Sci. Forum* **2017**, *880*, 95−98.
(41) Sriyanti, I.; Jauhari, J. Electrospun of Poly(Vinyl Alcohol) Nanofiber as Carrier of Garcinia Mangostana L. Pericarp Extract. *J. Phys.: Conf. Ser.* **2019**, *1170*, 012056.
(42) Taj, M.; Manohara, S. R.; Hanagodimath, S. M.; Gerward, L. Novel Conducting Poly(3,4-Ethylenedioxythiophene) − Graphene Nanocomposites with Gigantic Dielectric Properties and Narrow Optical Energy Band Gap. *Polym. Test.* **2020**, *90*, 106650.
(43) Thekkedath, J.; Bipinbal, P. K.; Thomas, T.; Narayanankutty, S. K. Polythiophene Coated Cellulosic Fibers from Banana Stem for Improved Electrical, Mechanical, Thermal and Dielectric Properties of Polypropylene Composites. *J. Sci. Res.* **2020**, *12*, 687−699.
(44) Pan, X.-r.; Wang, M.; Qi, X.-d.; Zhang, N.; Huang, T.; Yang, J.-h.; Wang, Y. Fabrication of Sandwich-Structured PPy/MoS2/PPy Nanosheets for Polymer Composites with High Dielectric Constant, Low Loss and High Breakdown Strength. *Compos. Appl. Sci. Manuf.* **2020**, *137*, 106032.
(45) Xi, X.; Chung, D. D. L. Colossal Electric Permittivity Discovered in Polyacrylonitrile (PAN) Based Carbon Fiber, with Comparison of PAN-Based and Pitch-Based Carbon Fibers. *Carbon N. Y.* **2019**, *145*, 734−739.
(46) Kambale, K. R.; Goyal, R.; Butee, S. P.; Parsewar, R.; Gawade, H.; Shroff, S. Novel Polyacrylonitrile/Potassium Sodium Niobate Composites with Superior Dielectric and Thermal Properties. *Compos. Commun.* **2017**, *5*, 8−12.
(47) Kausar, A. Polyacrylonitrile-Based Nanocomposite Fibers: A Review of Current Developments. *J. Plast. Film Sheeting* **2019**, *35*, 295−316.
(48) Palade, S.; Pantazi, A.; Vulpe, S.; Berbecaru, C.; Ţucureanu, V.; Oprea, O.; Negrea, R. F.; Dragoman, D. Tunable Dielectric Properties in Polyacrylonitrile/Multiwall Carbon Nanotube Composites. *Polym. Compos.* **2017**, *38*, 1741−1748.
(49) Huang, A.; Liu, F.; Cui, Z.; Wang, H.; Song, X.; Geng, L.; Wang, H.; Peng, X. Novel PTFE/CNT Composite Nanofiber Membranes with Enhanced Mechanical, Crystalline, Conductive, and Dielectric Properties Fabricated by Emulsion Electrospinning and Sintering. *Compos. Sci. Technol.* **2021**, *214*, 108980.
(50) Sriyanti, I.; Marlina, L.; Fudholi, A.; Marsela, S.; Jauhari, J. Physicochemical Properties and in Vitro Evaluation Studies of Polyvinylpyrrolidone/Cellulose Acetate Composite Nanofibres Loaded with Chromolaena Odorata (L) King Extract. *J. Mater. Res. Technol.* **2021**, *12*, 333−342.
(51) Nasir, S.; Hussein, M. Z.; Yusof, N. A.; Zainal, Z. Oil Palm Waste-Based Precursors as a Renewable and Economical Carbon Sources for the Preparation of Reduced Graphene Oxide from Graphene Oxide. *Nanomaterials* **2017**, *7*, 1−18.
(52) Liu, S. D.; Li, D. S.; Yang, Y.; Jiang, L. Fabrication, Mechanical Properties and Failure Mechanism of Random and Aligned Nanofiber Membrane with Different Parameters. *Nanotechnol. Rev.* **2019**, *8*, 218−226.

https://doi.org/10.1021/acsomega.2c03144
ACS Omega 2022, 7, 33087−33096

(53) Samadian, H.; Mobasheri, H.; Hasanpour, S.; Majidi, R. F. Electrospinning of Polyacrylonitrile Nanofibers and Simulation of Electric Field via Finite Element Method. *Nanomed. Res. J.* **2017**, *2*, 87−92.
(54) Sriyanti, I.; Agustini, M. P.; Jauhari, J.; Sukemi, S.; Nawawi, Z. Electrospun Nylon-6 Nanofibers and Their Characteristics. *J. Ilm. Pendidik. Fis. Al-Biruni* **2020**, *9*, 9−19.
(55) Sriyanti, I.; Almafie, M. R.; Nugraha, Y. P.; Idjan, M. K. N. A.; Jauhari, J. The Morphology of Polyvinylpyrrolidone Nanofibers Containing Anredera Cordifolia Leaves. *J. Ilm. Pendidik. Fis. Al-Biruni* **2021**, *10*, 179−189.
(56) Waresindo, W. X.; Luthfianti, H. R.; Edikresnha, D.; Suciati, T.; Noor, F. A.; Khairurrijal, K. A Freeze-Thaw PVA Hydrogel Loaded with Guava Leaf Extract: Physical and Antibacterial Properties. *RSC Adv.* **2021**, *11*, 30156−30171.
(57) Jauhari, J.; Suharli, A. J.; Nawawi, Z.; Sriyanti, I. Synthesis and Characteristics of Polyacrylonitrile (PAN) Nanofiber Membrane Using Electrospinning Method. *J. Chem. Technol. Metall.* **2021**, *56*, 698−703.
(58) Mohd Abdah, M. A. A.; Zubair, N. A.; Azman, N. H. N.; Sulaiman, Y. Fabrication of PEDOT Coated PVA-GO Nanofiber for Supercapacitor. *Mater. Chem. Phys.* **2017**, *192*, 161−169.
(59) Castro-Muñoz, R.; Buera-González, J.; de la Iglesia, Ó.; Galiano, F.; Fíla, V.; Malankowska, M.; Rubio, C.; Figoli, A.; Téllez, C.; Coronas, J. Towards the Dehydration of Ethanol Using Pervaporation Cross-Linked Poly(Vinyl Alcohol)/Graphene Oxide Membranes. *J. Membr. Sci.* **2019**, *582*, 423−434.
(60) Faniyi, I. O.; Fasakin, O.; Olofinjana, B.; Adekunle, A. S.; Oluwasusi, T. V.; Eleruja, M. A.; Ajayi, E. O. B. The Comparative Analyses of Reduced Graphene Oxide (RGO) Prepared via Green, Mild and Chemical Approaches. *SN Appl. Sci.* **2019**, *1*, 1181.
(61) Strankowski, M.; Włodarczyk, D.; Piszczyk, Ł.; Strankowska, J. Polyurethane Nanocomposites Containing Reduced Graphene Oxide, FTIR, Raman, and XRD Studies. *J. Spectrosc.* **2016**, *2016*, 1−6.
(62) Habte, A. T.; Ayele, D. W.; Hu, M. Synthesis and Characterization of Reduced Graphene Oxide (RGO) Started from Graphene Oxide (GO) Using the Tour Method with Different Parameters. *Adv. Mater. Sci. Eng.* **2019**, *2019*, 5058163.
(63) Othman, F. E. C.; Yusof, N.; González-Benito, J.; Fan, X.; Ismail, A. F. Electrospun Composites Made of Reduced Graphene Oxide and Polyacrylonitrile-Based Activated Carbon Nanofibers (RGO/ACNF) for Enhanced CO2 Adsorption. *Polymers* **2020**, *12*, 2117.
(64) Wang, S.; Chi, H.; Chen, L.; Li, W.; Li, Y.; Li, G.; Ge, X. Surface Functionalization of Graphene Oxide with Polymer Brushes for Improving Thermal Properties of the Polymer Matrix. *Adv. Polym. Technol.* **2021**, *2021*, 5591420.
(65) Özkan, V.; Yapici, A.; Karaaslan, M.; Akgöl, O. Electromagnetic Scattering Properties of MWCNTs/Graphene Doped Epoxy Layered with PVC Nanofiber/E-Glass Composites. *J. Electron. Mater.* **2020**, *49*, 2249−2256.
(66) Zhao, H.; Wu, X.; Liu, Y.-g.; Cheng, B.; Huang, Z.; Fang, M.; Min, X. Processing Microstructure and Electrochemical Properties of Reduced Graphene Oxide Reinforced Carbon Nanofiber Formed by Gyration. *Chem. Phys. Lett.* **2021**, *767*, 138393.
(67) Sujiono, E. H.; Zurnansyah; Zabrian, D.; Dahlan, M. Y.; Amin, B. D.; Samnur; Agus, J. Graphene Oxide Based Coconut Shell Waste: Synthesis by Modified Hummers Method and Characterization. *Heliyon* **2020**, *6*, No. e04568.
(68) Fatmawati, D. A.; Triyono; Trisunaryanti, W.; Oktaviano, H. S.; Chasanah, U. The Study of Partially and Fully Oxidized Graphene Oxide Prepared by Green Synthesis for Wide-Scale Fabrication. *Rasayan J. Chem.* **2021**, *14*, 2129−2135.
(69) Ke, G.; Jin, X.; Hu, H. Electrospun Polyvinylidene Fluoride/Polyacrylonitrile Composite Fibers: Fabrication and Characterization. *Iran. Polym. J.* **2020**, *29*, 37−46.
(70) Duan, G.; Fang, H.; Huang, C.; Jiang, S.; Hou, H. Microstructures and Mechanical Properties of Aligned Electrospun Carbon Nanofibers from Binary Composites of Polyacrylonitrile and Polyamic Acid. *J. Mater. Sci.* **2018**, *53*, 15096−15106.
(71) Su, Y.; Zhang, W.; Lan, J.; Sui, G.; Zhang, H.; Yang, X. Flexible Reduced Graphene Oxide/Polyacrylonitrile Dielectric Nanocomposite Films for High-Temperature Electronics Applications. *ACS Appl. Nano Mater.* **2020**, *3*, 7005−7015.
(72) Gergin, I.; Ismar, E.; Sarac, A. S. Oxidative Stabilization of Polyacrylonitrile Nanofibers and Carbon Nanofibers Containing Graphene Oxide (GO): A Spectroscopic and Electrochemical Study. *Beilstein J. Nanotechnol.* **2017**, *8*, 1616−1628.
(73) Madakbaş, S.; Çelik, Z.; Dumludağ, F.; Kahraman, M. V. Preparation, Characterization and Electrical Properties of Polyacrylonitrile/Huntite Composites. *Polym. Bull.* **2014**, *71*, 1471−1481.
(74) Ghafari, E.; Feng, Y.; Liu, Y.; Ferguson, I.; Lu, N. Investigating Process-Structure Relations of ZnO Nanofiber via Electrospinning Method. *Compos. Part B Eng.* **2017**, *116*, 40−45.
(75) Dang, W.; Liu, J.; Wang, X.; Yan, K.; Zhang, A.; Yang, J.; Chen, L.; Liang, J. Structural Transformation of Polyacrylonitrile (PAN) Fibers during Rapid Thermal Pretreatment in Nitrogen Atmosphere. *Polymers* **2020**, *12*, 63.
(76) Karbownik, I.; Rac-Rumijowska, O.; Fiedot-Toboła, M.; Rybicki, T.; Teterycz, H. The Preparation and Characterization of Polyacrylonitrile-Polyaniline (PAN/PANI) Fibers. *Materials* **2019**, *12*, 664.
(77) Liu, Y.; Peng, X.; Cao, Q.; Jing, B.; Wang, X.; Deng, Y. Gel Polymer Electrolyte Based on Poly(Vinylidene Fluoride)/Thermoplastic Polyurethane/Polyacrylonitrile by the Electrospinning Technique. *J. Phys. Chem. C* **2017**, *121*, 19140−19146.
(78) Saiful Badri, M. A.; Salleh, M. M.; Md Noor, N. F.; Rahman, M. Y. A.; Umar, A. A. Green Synthesis of Few-Layered Graphene from Aqueous Processed Graphite Exfoliation for Graphene Thin Film Preparation. *Mater. Chem. Phys.* **2017**, *193*, 212−219.
(79) Ain, Q. T.; Haq, S. H.; Alshammari, A.; Al-Mutlaq, M. A.; Anjum, M. N. The Systemic Effect of PEG-NGO-Induced Oxidative Stress in Vivo in a Rodent Model. *Beilstein J. Nanotechnol.* **2019**, *10*, 901−911.
(80) Ban, F. Y.; Majid, S. R.; Huang, N. M.; Lim, H. N. Graphene Oxide and Its Electrochemical Performance. *Int. J. Electrochem. Sci.* **2012**, *7*, 4345−4351.
(81) Tas, S.; Kaynan, O.; Ozden-Yenigun, E.; Nijmeijer, K. Polyacrylonitrile (PAN)/Crown Ether Composite Nanofibers for the Selective Adsorption of Cations. *RSC Adv.* **2016**, *6*, 3608−3616.
(82) Karbownik, I.; Fiedot, M.; Rac, O.; Suchorska-Woźniak, P.; Rybicki, T.; Teterycz, H. Effect of Doping Polyacrylonitrile Fibers on Their Structural and Mechanical Properties. *Polymer* **2015**, *75*, 97−108.
(83) Eivazi Zadeh, Z.; Solouk, A.; Shafieian, M.; Haghbin Nazarpak, M. Electrospun Polyurethane/Carbon Nanotube Composites with Different Amounts of Carbon Nanotubes and Almost the Same Fiber Diameter for Biomedical Applications. *Mater. Sci. Eng. C* **2021**, *118*, 111403.
(84) Koduru, H. K.; Marino, L.; Scarpelli, F.; Petrov, A. G.; Marinov, Y. G.; Hadjichristov, G. B.; Iliev, M. T.; Scaramuzza, N. Structural and Dielectric Properties of NaIO4—Complexed PEO/PVP Blended Solid Polymer Electrolytes. *Curr. Appl. Phys.* **2017**, *17*, 1518−1531.
(85) Liu, H.; Zhang, S.; Yang, J.; Ji, M.; Yu, J.; Wang, M.; Chai, X.; Yang, B.; Zhu, C.; Xu, J. Preparation, Stabilization and Carbonization of a Novel Polyacrylonitrile-Based Carbon Fiber Precursor. *Polymers* **2019**, *11*, 1150.
(86) Cho, S.; Kim, M.; Lee, J. S.; Jang, J. Polypropylene/Polyaniline Nanofiber/Reduced Graphene Oxide Nanocomposite with Enhanced Electrical, Dielectric, and Ferroelectric Properties for a High Energy Density Capacitor. *ACS Appl. Mater. Interfaces* **2015**, *7*, 22301−22314.
(87) Szepcsik, B.; Pukánszky, B. The Mechanism of Thermal Stabilization of Polyacrylonitrile. *Thermochim. Acta* **2019**, *671*, 200−208.
(88) Zhu, J.; Li, Q.; Che, Y.; Liu, X.; Dong, C.; Chen, X.; Wang, C. Effect of Na2CO3 on the Microstructure and Macroscopic Properties

https://doi.org/10.1021/acsomega.2c03144
ACS Omega 2022, 7, 33087−33096

and Mechanism Analysis of PVA/CMC Composite Film. *Polymers* **2020**, *12*, 453.
(89) Mo, Y.; Yang, L.; Zou, T.; Hou, W.; Liao, R. Preparation of Composite Insulating Paper with Decreased Permittivity, Good Mechanical and Thermal Properties by Kevlar/Nano Cellulose Fibrils/Softwood Pulp Hybrid. *IEEE Access* **2019**, *7*, 104258−104268.
(90) Li, H.; Xu, C.; Chen, Z.; Jiang, M.; Xiong, C. Graphene/Poly(Vinylidene Fluoride) Dielectric Composites with Polydopamine as Interface Layers. *Sci. Eng. Compos. Mater.* **2017**, *24*, 327−333.
(91) Chong, M. Y.; Evyan, Y. C. Y.; Zebardastan, N.; Kumar, K.; Ramesh, K.; Ramesh, S. Doping of Erbium(III) Oxide Nanoparticles−Polymer Interfaces in Biodegradable Inorganic Solid Polymer Electrolytes for Enhanced Ionic Conductivity. *Int. J. Nanoelectron. Mater.* **2020**, *13*, 119−128.
(92) Ishaq, S.; Kanwal, F.; Atiq, S.; Moussa, M.; Azhar, U.; Losic, D. Dielectric Properties of Graphene/Titania/Polyvinylidene Fluoride (G/TiO2/PVDF) Nanocomposites. *Materials* **2020**, *13*, 205.
(93) Anwar, N.; Ishtiaq, M.; Shakoor, A.; Niaz, N. A.; Rizvi, T. Z.; Qasim, M.; Irfan, M.; Mahmood, A. Dielectric Properties of Polymer/Clay Nanocomposites. *Polym. Polym. Compos.* **2021**, *29*, 807−813.
(94) Pan, Z.; Yao, L.; Zhai, J.; Shen, B.; Wang, H. Significantly Improved Dielectric Properties and Energy Density of Polymer Nanocomposites via Small Loaded of BaTiO3 Nanotubes. *Compos. Sci. Technol.* **2017**, *147*, 30−38.
(95) Khan, S.; Zulfiqar; Khan, T.; Khan, R.; Khan, M.; khattak, S. A.; khan, G. Investigation of Structural, Optical, Electrochemical and Dielectric Properties of SnO2/GO Nanocomposite. *J. Mater. Sci. Mater. Electron.* **2019**, *30*, 10202−10210.
(96) Jin, Y.; Gwak, Y.; Gerhardt, R. A. Effects of Nanoparticles Size and Interactions on Dielectric Properties of Polymer Matrix Flexible Dielectric Nanocomposites. *Adv. Compos. Mater.* **2020**, *29*, 235−246.
(97) Zheng, X.; Yu, H.; Yue, S.; Xing, R.; Zhang, Q.; Liu, Y.; Zhang, B. Functionalization of Graphene and Dielectric Property Relationships in PVDF/Graphene Nanosheets Composites. *Int. J. Electrochem. Sci.* **2018**, *13*, 1−13.
(98) Kou, Y.; Zhou, W.; Xu, L.; Cai, H.; Wang, G.; Liu, X.; Chen, Q.; Dang, Z. M. Surface Modification of GO by PDA for Dielectric Material with Well-Suppressed Dielectric Loss. *High Perform. Polym.* **2019**, *31*, 1183−1194.

https://doi.org/10.1021/acsomega.2c03144
ACS Omega 2022, 7, 33087−33096